Improving Fault Location in Wind Farm Interconnection Lines through Fault Resistance Estimation

C. V. C. Grilo, M. J. B. B. Davi, L. S. Lessa, D. V. Coury, R. A. S. Fernandes

***Abstract*—Electric power systems are continuously evolving to meet the growing demand. International agreements aim to increase the share of sustainable energy sources, which enhances the relevance of inverter-based resources (IBRs) interconnection lines. However, in power grids with IBRs, protection systems face challenges due to the behavior of voltages and currents. While phasor-based fault location is widely used, it is significantly impacted by fault resistance. Thus, the present article proposes an approach that combines apparent impedance techniques with machine learning (ML), using data exclusively from the substation, to accurately estimate fault locations in IBRs interconnection lines. Initially, a ML-based approach estimates the fault resistance and applies a compensation factor to estimate the fault current. The approach proved promising, reducing average errors in the fault location task to less than 1% without requiring new meters in the system, communication structures between transmission line terminals, or meters with higher sampling frequencies.**

***Keywords*—Fault location, Impedance-based fault location, Inverter-based Resources, Machine learning.**

I. Introduction

In recent years, increasing electricity demand, declining availability of mineral coal, and the implementation of public policies promoting sustainable energy have led to greater reliance on renewable sources, such as solar and wind power, both based on Inverter-Based Resources (IBRs) [1]. Simultaneously, regulatory changes have heightened the need for more efficient maintenance strategies and faster power restoration. Service quality indicators, which assess outage frequency and average interruption duration, have become a primary focus for electric utilities. In this context, Fault Location (FL) methods are essential tools, as the accurate identification of fault distance and location enables technical teams to quickly pinpoint the fault location, reduce power outage duration, and ultimately improve power quality indicators [2].

FL methods have undergone significant transformations. The precursors were based on monitoring voltages and currents to estimate the apparent impedance [2]. However, these methods are affected by fault resistance. With advancements and the availability of high sampling rates, traveling wave-based methods were proposed [3]. The main advantage of these methods is to achieve lower errors and be less influenced by fault resistance [4]. Due to this characteristic, they could be applied to short lines if the required high sampling rates are met [5]. With advancements in cloud processing and data storage capabilities, Machine Learning (ML)-based methods have become increasingly important, reducing the need for high sampling rate meters [6].

Considering the increasing demand for renewable energy sources, interconnection lines with wind farms have gained ground in recent years. A major difficulty lies in ensuring that the FL process remains reliable despite variations in fault resistance, preventing inaccuracies to the estimations made by FL placed on the grid side [4]. Therefore, enhancing FL methods through fault resistance estimation can reduce errors, increasing the overall efficiency of fault management.

The authors in [7] present a multi-method approach for FL in interconnection lines with wind farms. The proposed approach selects the best method based on the fundamental frequency component, depending on the type of fault. Based on [8], a modification of the Takagi zero-sequence method was proposed, considering new loop quantities applied to this method and enabling lower errors for phase-phase-ground faults. Although the method minimizes errors by selecting the best approach for each fault, higher errors are obtained when the fault resistance is high.

Conversely, traveling wave-based methods, as discussed in [9], are also used for FL in wind farm interconnection lines, classified into single-ended and double-ended approaches. However, frequencies in the MHz order are required and communication channel shortcomings persist.

Given the limitations imposed on classical methods and the constraints of traveling wave-based ones, the authors in [10] introduced an approach that combines fundamental component-based methods with ML techniques for FL in IBR-based systems. They used voltage and current phasors, symmetrical components, and distance estimation of existing methods based on the approach proposed in [7]. Although it

The authors would like to thank the Coordination for the Improvement of Higher Education Personnel- Brazil (CAPES) - Finance Code 001, the National Council for Scientific and Technological Development (CNPq) [402334/2023-0], and the Sao Paulo Research Foundation (FAPESP) [#2022/00483-0]. They also gratefully acknowledge the support of the RCGI – Research Centre for Greenhouse Gas Innovation, hosted by the University of São Paulo (USP), sponsored by FAPESP – São Paulo Research Foundation [#2020/15230-5], and sponsored by TotalEnergies, and the strategic importance of the support given by ANP (Brazil's National Oil, Natural Gas and Biofuels Agency) through the R&DI levy regulation. C. V. C. Grilo is with the University of São Paulo, São Carlos, Brazil (e-mail of corresponding author: caio.vinicius@usp.br). M. J. B. B. Davi, L. S. Lessa, D. V. Coury, and R. A. S. Fernandes are with the University of São Paulo, São Carlos, Brazil (e-mails: moisesdavi@usp.br; leonardolessa@usp.br; coury@sc.usp.br; ricardo.asf@usp.br).

Paper submitted to the International Conference on Power Systems Transients (IPST2025) in Guadalajara, Mexico, June 8-12, 2025.

reduces the FL error, the method relies solely on using ML, which requires prior training.

In this context, acknowledging that FL in systems with IBRs still demands further analysis and error reduction solutions, this work contributes to the state-of-the-art by presenting the following advancements:

- Developing a methodology for compensating fault resistance, which enables the reduction of errors in FL based on fundamental frequency components;
- Performing a comparative evaluation with existing phasor-based methods, aimed at highlighting the superiority of the proposed methodology in reducing FL;
- A fault resistance estimation method that can be used to predict the nature of the fault, enabling enhanced awareness for the maintenance team.

The structure of this article is organized as follows. Section II reviews the state-of-the-art classical FL methods based on the fundamental component. Section III presents the test system that represents typical wind farm interconnection topologies. Section IV presents the proposed methodology for FL in IBR interconnection lines through a fault resistance compensation factor. Section V presents the results and discussion. Finally, Section VI provides the conclusions of this article.

II. State-of-The-Art for Fault Location

Phasor-based methods were selected in this section as they require low sampling frequencies and are usually embedded in commercial devices. Furthermore, only methods that rely on measurements from a single Transmission Line (TL) terminal were considered as the proposed solution follows this approach. Furthermore, it is an approach that does not require communication infrastructure between the line terminals. Finally, priority was given to methods that adequately operate on all types of faults.

A. Impedance-based Method (IMPE)

This method is a precursor of phasor-based fault location methods [2], and its operation is based on the indirect measurement of the fault distance based on calculating the positive sequence impedance between the measurement and fault points. The fault location estimation in p.u. (m) is characterized by:

$$m = Real\left[\frac{\overrightarrow{V_l}/\overrightarrow{I_l}}{Z_{1L}}\right], \tag{1}$$

where $\overrightarrow{V_l}$ is the voltage loop and $\overrightarrow{I_l}$ the current loop as described in [7], and Z_{1L} is the positive sequence impedance of the TL.

The IMPE method is based on a fundamental equation that governs phasor-based fault location algorithms with measurements taken at only one TL end. However, this approach has significant limitations as parameters such as fault resistance, load current, TL capacitive effect, and system homogeneity directly impact its performance [2].

B. Reactance-based Method (REAC)

The algorithm is similar to IMPE. However, REAC minimizes the influence of fault resistance in the FL estimation by considering only the reactive component of the estimated impedance between the measurement and fault points. The accuracy of this method depends on the equivalence between the source angle and the fault current angle [11]. The following equation characterizes the distance estimated by REAC in p.u.:

$$m = \frac{Imag\left[\frac{\overrightarrow{V_l}}{\overrightarrow{I_l}}\right]}{Imag[Z_{1L}]}. \tag{2}$$

It is important to note that aspects such as the system´s non-homogeneity and the capacitive effect of the TL still impact the estimations.

Although the REAC improves the IMPE method, its accuracy in estimating the fault location is significantly affected when the fault currents from both TL terminals are not in phase. This phase mismatch can occur due to the presence of the system load during the fault or due to the non-homogeneity of the system. In these cases, an additional reactance besides the faulted line section is measured, impacting the fault position estimation. Furthermore, the TL capacitive effect also impacts these estimations [11].

C. Takagi Method (TAKS)

The TAKS method was proposed by [12] to improve the REAC, considering incremental currents in its decision process to reduce the effects of the load current on the fault location. The method requires both pre-fault and fault information to calculate incremental currents. This information is readily available on most commercial relays. The estimated fault location, in p.u., can be defined by:

$$m = \frac{Imag[\overrightarrow{V_l}\Delta\overrightarrow{I_l^*}]}{Imag[Z_{1L}\overrightarrow{I_l}\Delta\overrightarrow{I_l^*}]}, \tag{3}$$

where $\Delta\overrightarrow{I_l}$ is the incremental current determined by subtracting the fault samples from the pre-fault ones [12].

However, although the TAKS method represents an improvement of the REAC method by minimizing the influence of the system's load current on the fault distance estimation, the non-homogeneity of transmission systems, load variations before and during faults, and the TL capacitive effects still have a direct impact on its performance [12].

III. Test Power System Setup

The single-line diagram of the test system under consideration is shown in Fig. 1. The test system comprises a source with positive-sequence impedance $Z_1 = 0.112 + j6.3998\,[\Omega]$ and zero-sequence impedance $Z_0 = 0.435 + j18.3991\,[\Omega]$, along with a voltage level of 69 kV. The A-B line has impedances $Z_1 = 0.159 + j0.5003\,[\Omega/\text{km}]$ and $Z_0 = 0.516 + j1.5\,[\Omega/\text{km}]$, and capacitances $C_1 = 304.89\,[M\Omega \cdot m]$ and $C_0 = 449.59\,[M\Omega \cdot m]$, with a length of 60 km [7]. The 3, 4, and 5 km overhead lines were modelled using the π circuit without considering zero-sequence mutual coupling,

as they are directed to geographically distinct locations and have short lengths. The impedances of these lines are $Z_1 = 0.1098 + j0.3751$ [Ω/km] and $Z_0 = 0.2842 + j1.8597$ [Ω/km]. The transformer is of type Ynd1, rated at 5.2 MVA with 10% impedance. The wind turbine has a rated power of 4.2 MVA, utilizes a Full-Converter topology, and its control settings are adjusted as described in [13].

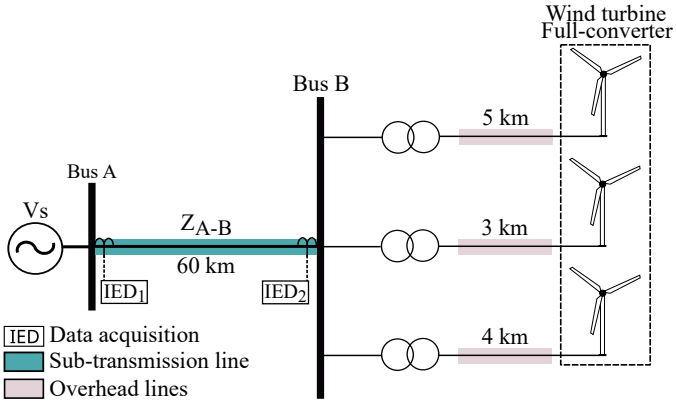

Fig. 1. Test system single-line diagram.

This system was chosen to represent the topology of interconnection lines in wind farms, that is, using uniform single-span TLs and transformers connected in a grounded star configuration on the grid side [10]. The sub-transmission line connects bus A to bus B. At bus A, a source is connected as a Thévenin equivalent representing the grid. At bus B, the collector lines of the wind farm are considered. Intelligent Electronic Devices (IEDs) were allocated at busbars A and B to acquire three-phase voltage and current signals, originating from bus A (IED_1) and bus B (IED_2). The study initially used only data from IED_1 to evaluate the performance of the FL method from the Transmission System Operator's point of view. Subsequently, a preliminary analysis was conducted using only data from IED_2, which is the measurement point with the highest influence from the atypical fault currents of IBR. The analysis aimed to assess the ability to compensate for the influence of fault resistance, initially testing all methods with data from IED_1 and subsequently with data from IED_2.

This power system was modelled and simulated using the PSCAD/EMTDC software with a sampling rate of 512 samples per cycle and considering fault parameters such as resistance, inception angle, type, and distance. A total of 17,850 simulated scenarios were used for training and validation, while 9,750 simulated scenarios were used for testing purposes. For training, the fault resistances considered were 0, 10, 25, and 50 Ω, while for testing, the values were 2, 8, 15, and 40 Ω. The fault inception angles for training were 0°, 45°, and 90°, and for testing, 35°, 55°, and 85°. The fault types included phase-ground (PG), phase-phase (PP), phase-phase-ground (PPG), and phase-phase-phase (PPP). Fault distances were selected every 500 meters for training and every 1,200 meters for testing.

IV. Improved FL method

The proposed routine is illustrated in Fig. 2. Each step of the method is detailed in the following subsections.

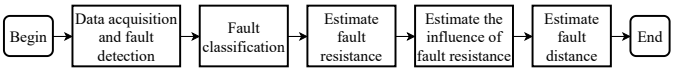

Fig. 2. Flowchart of the proposed approach.

A. Data acquisition and fault detection

The voltage and current signals for each phase are acquired at the substation and stored in a rotating buffer of three cycles. Due to the existence of fault detection methods already described in the literature, with accuracy rates greater than 99.9%, this step has not been detailed in this article [14]. After the fault is detected, the algorithm waits for two more cycles and locks the rotating buffer. Subsequently, the phasors of the first and third cycles are obtained.

B. Fault classification

Fault classification algorithms are well established in the literature. In [15], a methodology that utilizes voltages and currents from a single terminal, considering the grid side, classifies faults within a quarter cycle, achieving over 99% accuracy. In [16], a proposed method performs classification with more than 99.5% accuracy, considering measurements on the IBR side. In this article, it is assumed that the classification step was executed correctly.

C. Fault resistance estimation

Estimating fault resistance is challenging, and some authors have proposed methods for this estimation [17], [18]. In this context, as an additional contribution of this article, the potential of ML methods has been investigated for the task of estimating fault resistance. For this purpose, the Waikato Environment for Knowledge Analysis (WEKA) software [19] was utilized, which already encompasses a robust collection of ML methods and several features that aided the conducted investigations. The software provides five main categories of regression/classification methods: Functions, Lazy, Meta, Rules, and Trees [19]. For the preliminary analysis, 26 methods from these categories were pre-selected based on their descriptions in WEKA and are presented below:

- **Functions Class:** Gaussian Processes (GP), Linear Regression, Multilayer Perceptron, Simple Linear Regression, SMOreg;
- **Lazy Class:** IBk (KNN), KStar (K*), LWL;
- **Meta Class:** Additive Regression, Bagging (BAG), Multi Scheme, Random Committee (RC), Randomizable Filtered Classifier, Random Sub Space (RSS), Regression By Discretization, Stacking, Vote, Weighted Instances Handler Wrapper;
- **Rules Class:** Decision Table, M5 Rules (M5R), Zero R;
- **Trees Class:** Decision Stump, M5P, Random Forest (RF), Random Tree, REP Tree (REPT).

It is noteworthy, since this is an investigation of potential, the default parameter settings of the ML methods in WEKA

were considered, as optimizing these parameters for each of the evaluated methods is not within the scope of this work.

The application of WEKA consisted of three main steps to determine the most suitable ML method. The steps undertaken are described as follows:

- **Selection of the ML method** – For each method described above, the training and validation set was selected with the voltage and current phasors for each phase, obtained in the second cycle after the fault;
- **Training and validation** – The training and validation process used cross-validation with 5 folds;
- **Testing** – Once the method was trained and validated, a separate subset, referred to as the test set, was loaded. The result obtained from WEKA was the Mean Absolute Error (MAE), $MAE = \sum_{i=1}^{n} |R_f - \hat{R_f}|/n$ where R_f is the actual fault resistance, $\hat{R_f}$ is the estimated resistance, and n is the number of instances. This metric is widely used in fault location problems [10].

Table I compares each fault type's top ten ML methods. The analysis shows that RSS had the best performance with a MAE of 4.58 Ω, followed by RF at 4.67 Ω. Given the minimal difference and RF's superior performance for single-phase faults, subsequent stages will utilize the RF method with WEKA's default parameters.

TABLE I
EVALUATION OF MAES FROM THE TEN BEST ML METHODS FOR ESTIMATING FAULT RESISTANCE, DIVIDED BY FAULT TYPE.

Ref	Method	Fault Type			
		PG MAE [Ω]	PPG MAE [Ω]	PP MAE [Ω]	PPP MAE [Ω]
[20]	GP	4.06	5.55	7.88	11.04
[21]	KNN	6.12	6.52	6.01	8.66
[22]	K*	4.93	5.46	6.02	6.03
[23]	BAG	5.82	6.18	7.44	6.29
[24]	RC	4.15	4.93	5.77	5.55
[25]	RSS	3.99	3.98	4.85	5.50
[26]	M5R	5.89	6.44	7.94	8.40
[27]	M5P	5.78	6.55	7.26	9.12
[28]	RF	3.93	4.11	5.30	5.33
[29]	REPT	6.20	6.51	7.91	8.21

D. Estimate the influence of fault current

The methods presented are affected by fault resistance. Even methodologies aimed at minimizing this influence, whether through the imaginary part or compensation factors, face issues due to current variations caused by the resistance, which can lead to errors.

When a fault occurs in the line between buses A and B, as shown in Fig. 3.

The impedance seen from bus A can be calculated according to (4):

$$Z_{app} = \frac{\overrightarrow{V_l}}{\overrightarrow{I_l}} = Z_{LA} + \frac{I_F}{\overrightarrow{I_l}} \times R_F, \tag{4}$$

where $\overrightarrow{V_l}$ is the voltage at bus A during the fault, $\overrightarrow{I_l}$ is the current from bus A, I_F is the current through the fault

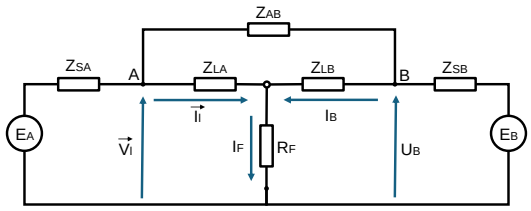

Fig. 3. Example of a fault configuration between two buses.

resistance R_F, and Z_{LA} is the line impedance between bus A and the fault point.

During the fault, the total fault current $\overrightarrow{I_l}$ is a function of the current flowing through the fault and the current flowing towards the load, as shown in (5):

$$\overrightarrow{I_l} = I_F + I_{pre}, \tag{5}$$

where I_F is the current flowing through the fault resistance and I_{pre} is the current flowing to the load before the fault.

Finally, only the fault current can be obtained as a part of $\overrightarrow{I_l}$, as shown in (6):

$$I_F = \mathbf{k} \times \overrightarrow{I_l}, \tag{6}$$

where $\mathbf{k} = ke^{j\gamma}$ is a complex factor for pure fault current distribution.

According to [30], the distribution factor $\mathbf{k}$ does not depend on the magnitudes or phases of the voltages at the line terminals but only on the grid topology. According to the authors, this factor is calculated as shown in (7):

$$\mathbf{k} = \frac{(Z_{LB} + Z_{SB}) \times Z_{AB} + (Z_{SA} + Z_{SB}) \times Z_{LB}}{Z_{SL} \times Z_{AB} + (Z_{LA} + Z_{LB})(Z_{SA} + Z_{SB})}, \tag{7}$$

where $Z_{SL} = Z_{SA} + Z_{SB} + Z_{LA} + Z_{LB}$. Thus, according to (4) to (7), the apparent impedance seen from point A can be written as shown in (8):

$$Z = Z_{LA} + \frac{R_f}{k} \times \left(\frac{\overrightarrow{I_l} - I_{pre}}{\overrightarrow{I_l} \times e^{j\gamma}} \right). \tag{8}$$

The signals locally available at one end of the line, in this case considering end A, are $\overrightarrow{V_l}$, $\overrightarrow{I_l}$, and I_{pre}. Thus, it is possible to calculate the apparent impedance Z_A and also determine the current ratio $(\overrightarrow{I_l} - I_{pre})/\overrightarrow{I_l}$. Moreover, as shown in [30], it can be assumed that the phase angle γ is usually less than 10° and the fault resistance has been previously estimated. In this way, a compensation factor can be defined as shown in (9):

$$\beta = \frac{\Delta \overrightarrow{I_l}}{k \times \overrightarrow{I_l}}. \tag{9}$$

Finally, the behavior of the four types of faults was analyzed, and the compensation values were determined through the process of minimizing quadratic errors so that the factor k remained constant for each type of fault, as shown in Table II.

TABLE II
COMPENSATION FACTOR β VALUES.

Fault type	Compensation factor
AG	$[(\vec{I}_{fa} + k0*\vec{I}_{f0}) - I_{a_{pre}}]/(\vec{I}_{fa} + k0*\vec{I}_{f0})$
BG	$[(\vec{I}_{fb} + k0*\vec{I}_{f0}) - I_{b_{pre}}]/(\vec{I}_{fb} + k0*\vec{I}_{f0})$
CG	$[(\vec{I}_{fc} + k0*\vec{I}_{f0}) - I_{c_{pre}}]/(\vec{I}_{fc} + k0*\vec{I}_{f0})$
AB - ABG	$[(\vec{I}_{fa} - \vec{I}_{fb}) - (I_{a_{pre}} - I_{b_{pre}})]/[3(\vec{I}_{fa} - \vec{I}_{fb})]$
BC - BCG	$[(\vec{I}_{fb} - \vec{I}_{fc}) - (I_{fb_{pre}} - I_{fc_{pre}})]/[3(\vec{I}_{fb} - \vec{I}_{fc})]$
CA - CAG	$[(\vec{I}_{fc} - \vec{I}_{fa}) - (I_{fc_{pre}} - I_{fa_{pre}})]/[3(\vec{I}_{fc} - \vec{I}_{fa})]$
ABC-G	$-[(\vec{I}_{fa} - \vec{I}_{fb}) - (I_{a_{pre}} - I_{b_{pre}})]/[3(\vec{I}_{fa} - \vec{I}_{fc})]$

E. Fault distance estimation

Based on the apparent impedance method shown in [2], it is possible to find a dependency with fault resistance, as presented in (10):

$$m = \frac{\vec{V}_l - R_f I_f}{Z_{L1}\ \vec{I}_l}. \tag{10}$$

From the propositions presented in [11], it is suggested to use the imaginary part of the impedance to minimize the influence of fault resistance. The logic is that fault resistance primarily affects the real part of the impedance, while the imaginary part, related to reactance, remains less affected.

On the other hand, the authors in [12] present an alternative approach to minimize errors in locating faults, considering the current variation. The proposed methodology employs the estimation of fault resistance, $\hat{R}_f$, as a compensation factor using the presented ML algorithms. Specifically, $\hat{R}_f$ was estimated using the Random Forest algorithm, following the detailed process outlined in previous sections and configured according to the parameters established in [19].

In (11), the proposed equation is presented to estimate the fault distance per unit length. To reduce the influence of fault resistance, the term $\beta\hat{R}_f$ is included, which represents the estimated contribution of fault resistance adjusted by a correction factor, β. The application of the imaginary part further mitigates the impact of fault resistance.

$$m = \frac{Imag\left(\frac{\vec{V}_l}{\vec{I}_l} - \beta\hat{R}f\right)}{Imag(Z_{L1})}. \tag{11}$$

V. EVALUATING THE PROPOSED METHODOLOGY AGAINST TRADITIONAL METHODS

This section presents the metrics used for the method comparison, followed by general comparisons by fault type. The influence of fault resistance on the methods is then analyzed. Finally, a general comparison of the results is provided.

A. Performance evaluation metrics

In distance-based fault locators, it is common to adopt the Mean Relative Error (MRE) [5]. This metric accounts for the difference between the actual distance and the estimated distance of the fault relative to the line length. In this study, the MRE was evaluated using (12), considering a set of *n* cases and the total length of the monitored line.

$$MRE\ [\%] = \sum_{i=1}^{n} \frac{\left(\frac{|D-\hat{D}|}{L}\right)}{n} \times 100, \tag{12}$$

where *D* represents the actual fault distance, $\hat{D}$ is the estimated distance, and *L* is the length of the monitored line.

B. Comparison of methods by fault type

An analysis based on the fault types was conducted. Tables III to VI present the results for each fault type as a function of fault resistance, considering both classical and proposed methods.

Table III shows the results for PG faults. Considering the lowest fault resistance, there is no significant difference between the proposed and classical methods. However, as the resistance increases, a greater advantage of using the proposed methods compared to the other approaches can be observed. For faults with a resistance of 15 Ω, the MRE is 17.39% for the impedance-based method, 2.97% for the reactance method, 0.95% for the TAKS method, and remains at 0.50% for the proposed method. For a fault resistance of 40 Ω, the MRE of the TAKS method reached 2.42%, while that of the proposed method was 0.95%. This result highlights the superiority of the proposed method over classical ones, particularly in scenarios with high fault resistance.

TABLE III
COMPARISON OF MRE FOR DIFFERENT FAULT RESISTANCES AND METHODS ANALYZED IN PG FAULTS.

	Method			
Resistance [Ω]	IMPE MRE [%]	REAC MRE [%]	TAKS MRE [%]	**Proposed** MRE [%]
2 Ω	3.05	0.68	0.56	**0.55**
8 Ω	9.42	1.59	0.54	**0.28**
15 Ω	17.39	2.97	0.95	**0.50**
30 Ω	35.78	6.28	1.73	**0.85**
40 Ω	48.87	8.57	2.42	**0.95**

The results for PPG faults are presented in Table IV. The reactance method outperformed the TAKS method for this fault type, achieving an MRE of 0.56% compared to 0.66%. Similar to what was observed for PG faults, the proposed method showed a smaller reduction in errors in scenarios with lower impedances. However, for higher fault resistances, such as 40 Ω, while the TAKS method achieved an MRE of 5.92% and the reactance method 2.78%, the proposed method reduced the MRE to 1.08%, leading to a 61.15% reduction in location errors. In absolute terms, this improvement corresponds to a decrease in the search area from 1,668 meters to 648 meters.

The results for PP faults are presented in Table V. As previously observed, all analyzed methods exhibited reduced errors for fault resistances of 2 Ω. However, as the resistance increases, the proposed method demonstrates superior performance. For resistances of 8 Ω and 15 Ω, the error reduction was 15.21% and 63.63%, respectively. In faults

TABLE IV
COMPARISON OF MRE FOR DIFFERENT FAULT RESISTANCES AND METHODS ANALYZED IN PPG FAULTS.

Resistance [Ω]	Method IMPE MRE [%]	REAC MRE [%]	TAKS MRE [%]	**Proposed** MRE [%]
2 Ω	2.89	0.56	0.66	**0.56**
8 Ω	8.70	0.54	1.80	**0.66**
15 Ω	16.52	0.67	2.77	**0.74**
30 Ω	34.73	1.71	4.63	**0.81**
40 Ω	47.84	2.78	5.92	**1.08**

with a resistance of 30 Ω, the TAKS method presented an MRE of 1.46%, whereas the proposed method reduced this value to 0.39%. In the case of 40 Ω, the TAKS method achieved an MRE of 1.95%, while the proposed method obtained 0.51%, resulting in a 73.84% improvement in fault location accuracy. In absolute terms, while the TAKS method presents an average error of approximately 1,200 meters, the proposed method reduces this error to only 300 meters. These results confirm the advantage of the proposed method for fault location in scenarios with higher fault resistances.

TABLE V
COMPARISON OF MRE FOR DIFFERENT FAULT RESISTANCES AND METHODS ANALYZED IN PP FAULTS.

Resistance [Ω]	Method IMPE MRE [%]	REAC MRE [%]	TAKS MRE [%]	**Proposed** MRE [%]
2 Ω	1.81	0.72	0.74	**0.72**
8 Ω	4.94	0.58	0.46	**0.39**
15 Ω	8.70	0.86	0.66	**0.24**
30 Ω	17.13	1.55	1.46	**0.39**
40 Ω	23.05	2.11	1.95	**0.51**

The results for the PPP faults are presented in Table VI. Although the impedance method exhibited a lower error compared to the proposed method for faults of 2 Ω, for faults of 15 Ω the proposed method achieved 0.44%, surpassing the reactance and TAKS methods, which obtained 1.36% and 2.38%, respectively. As previously analyzed, for faults of 40 Ω, the proposed method reduced the mean error by 65.14%, reaching an MRE of 0.99%.

TABLE VI
COMPARISON OF MRE FOR DIFFERENT FAULT RESISTANCES AND METHODS ANALYZED IN PPP FAULTS.

Resistance [Ω]	Method IMPE MRE [%]	REAC MRE [%]	TAKS MRE [%]	**Proposed** MRE [%]
2	0.41	0.90	1.16	**0.75**
8	2.11	1.04	1.65	**0.53**
15	4.08	1.36	2.38	**0.44**
30	8.23	2.27	4.20	**0.68**
40	11.16	2.84	5.36	**0.99**

An analysis of the maximum observed errors was conducted. Table VII presents the highest MRE obtained for each type of fault, while Fig. 4 illustrates this variation, providing a comparative view of each method's performance. For PG faults, the proposed method reduced the maximum error by 63.62%, achieving an MRE of 3.54%. For PPG faults, the reduction was 14.47%, with an MRE of 3.96%. In PP faults, the method reduced by 54.74%, resulting in a maximum MRE of 1.48%. Finally, for PPP faults, the maximum error reduction was 69.55%, reaching an MRE of 1.76%.

TABLE VII
COMPARISON OF MAXIMUM MRE FOR DIFFERENT FAULT TYPE.

Fault Type	Method IMPE MRE [%]	REAC MRE [%]	TAKS MRE [%]	**Proposed** MRE [%]
PG	72.21	10.71	9.73	**3.54**
PPG	50.36	4.63	12.99	**3.96**
PP	24.84	3.27	3.64	**1.48**
PPP	13.95	5.78	10.13	**1.76**

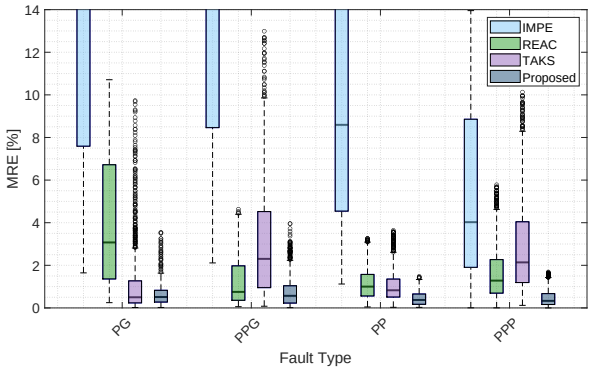

Fig. 4. Comparison of methods by fault types.

C. Comparison based on fault resistance

Phasor measurement-based methods, using data from a single terminal, usually encounter difficulties in fault location when the fault resistance is high. In Fig. 5, the influence of fault resistance was evaluated for both the reviewed methods and the proposed one.

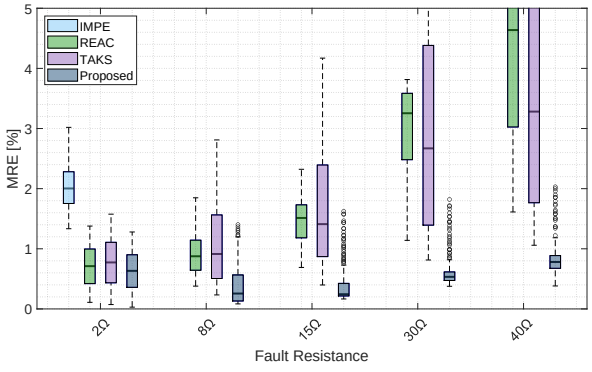

Fig. 5. Comparison of methods under different fault resistances.

Considering the fault scenarios evaluated in the test system, the fault resistance varied from 2 to 40 Ω. For the case of

2 Ω, the impedance method exhibited an MRE close to 2%, while the reactance, TAKS, and proposed methods achieved MREs near 0.5%. For faults with 5 Ω, the impedance method recorded MREs exceeding 5%, whereas the reactance and TAKS methods had values close to 1%, and the proposed method maintained an MRE below 0.5%.

The results for fault resistances above 15 Ω confirmed the effectiveness of the proposed method. Reviewed methods exhibited MREs greater than 2%, whereas the proposed method remained below 0.5%. For 40 Ω, the REAC method showed an MRE exceeding 4%, and the TAKS surpassed 3%, while the proposed method remained below 1%.

In addition to the MRE, an analysis of the estimated average errors in meters was conducted, as presented in Table VIII. For faults with a resistance of 2 Ω, the classical methods resulted in an average error of 500 meters, while the proposed method reduced this error to 390 meters. For faults of 8 Ω, the reactance-based method presented an error of 564 meters, whereas the proposed method reduced this discrepancy to 282 meters. For resistances of 30 Ω, the traditional methods recorded an average error of 1,770 meters, while the proposed method reduced this value to 408 meters. For faults of 40 Ω, the classical methods resulted in an average error of 2,346 meters, while the proposed method reduced to 528 meters.

TABLE VIII
COMPARISON OF THE ESTIMATED DISTANCE FOR EACH ANALYZED METHOD AS A FUNCTION OF FAULT RESISTANCE.

	Method			
Resistance [Ω]	IMPE Error [m]	REAC Error [m]	TAKS Error [m]	**Proposed** Error [m]
2	1,224	426	468	**390**
8	3,774	564	666	**282**
15	7,002	882	1014	**288**
30	14,382	1770	1806	**408**
40	19,638	2448	2346	**528**

The proposed method demonstrated a greater ability to mitigate the influence of fault resistance, ensuring higher accuracy even under high-resistance conditions. Additionally, it exhibited lower MRE variation and did not present outliers exceeding 2%, making it the most robust among the evaluated methods.

D. Overall results of the proposed fault locator

Overall, the proposed method utilizes only phasor data collected from a single system terminal, eliminating the need for multiple measurement points and data synchronization. As it is based on machine learning algorithms, a prior system-specific training phase is required, using post-fault phasor signals obtained through simulations. Minor system modifications that do not alter topology do not invalidate training, although they may reduce the accuracy of fault resistance estimation. In such cases, retraining can improve the predictive model's performance. Alternative methods, as presented in [17], can be employed as substitutes for the proposed machine learning-based approach in fault resistance estimation, although they typically offer lower accuracy.

Once trained, the proposed approach exhibits low computational complexity compared to approaches that require high sampling rates. As shown in Fig. 6, the overall MRE was reduced to less than 1%, representing a significant advancement for fundamental component-based methods using data from a single terminal. This level of accuracy is typically achieved only by high-frequency estimators with measurement equipment operating in the range of hundreds of kilohertz.

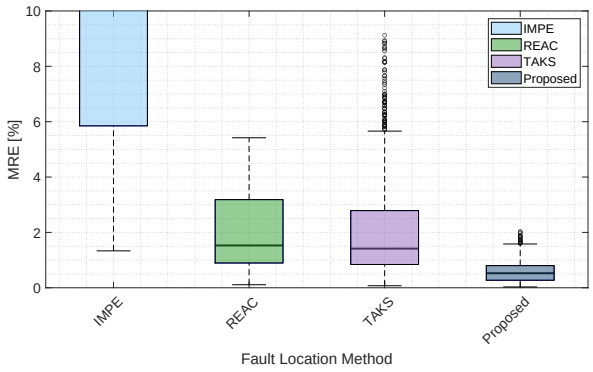

Fig. 6. Comparison of overall MRE obtained for state-of-the-art and proposed methods

E. Analysis considering IED_2 measurements

Initial studies were conducted for compensation on the IBR side (IED_2) in single-phase faults, considering the atypical characteristics of fault currents originating from this type of generation [10]. The fault resistance estimation process was replicated using IED_2 measurements with the Random Forest (RF) method, with an estimated MAE of 4.37 Ω, using the same parameters as before.

For this initial analysis, fault resistance values up to 15 Ω were considered. Table IX presents the average and maximum errors for this range. The best classical method analyzed, TAKS, showed an average error of 2.67%, while the proposed method reduced this value to 1.07%, decreasing the average error from 1,602 meters to 642 meters. The maximum error, which was 7.71% in the TAKS method, was reduced to 5.95%. The standard deviation was also reduced from 2.32 in the TAKS method to 1.58 in the proposed method, indicating less variation in accuracy.

TABLE IX
ANALYSIS OF THE MEAN AND MAXIMUM ERRORS FOR THE IBR SIDE, IED_2.

	Method			
	IMPE [MRE]	REAC [MRE]	TAKS [MRE]	**Proposed** [MRE]
MRE	7.7481	4.0110	2.6756	**1.0766**
Maximum	15.9089	21.8486	7.7127	**5.9558**

Scenarios for 40 Ω were also evaluated. In these cases, the maximum error of the TAKS method reached 52.78%, with a standard deviation of 11.03, while the proposed method reduced it to 27.21%, with a standard deviation of 8.06. It was concluded that the compensation factor is applicable to IED_2

measurements and may contribute to future studies aimed at reducing errors in faults with higher resistance.

VI. Conclusions

Accurately locating faults in interconnection lines remains a challenge due to the influence of fault resistance on impedance-based methods. Conventional FL approaches often neglect this parameter or struggle with its stochastic nature, leading to significant errors, particularly in high-resistance scenarios. To address this issue, this work proposed a novel FL methodology that integrates ML techniques with impedance-based methods to estimate and compensate for fault resistance.

The proposed approach was validated using a test system representative of wind farm interconnections, considering a wide range of fault conditions, including variations in resistance, inception angle, type, and distance. The results demonstrated that by incorporating fault resistance estimation, the method significantly improves FL accuracy, reducing errors by up to 78% for faults with 40 Ω compared to traditional techniques. Additionally, the methodology relies solely on voltage and current phasor measurements from a single terminal, eliminating the need for additional meters, communication infrastructure, or high-sampling-rate devices, making it practical for real-world deployment.

Beyond fault location, the ability to estimate fault resistance provides valuable insights into fault characteristics, which can support protection and maintenance strategies. This study also highlighted the potential of ML in enhancing FL methods, paving the way for future research. As the next steps, further optimizations of ML algorithms should be explored to enhance accuracy and computational efficiency. Finally, by improving fault location accuracy in interconnection lines, the proposed method contributes to more reliable and resilient power systems, reducing outage durations and supporting integrating renewable energy into modern power networks.

References

[1] J. Lee and F. Zhao, *Global Wind Report 2024*. Brussels, BE: GWEC, 2024.

[2] G. Ziegler, *Numerical Distance Protection: Principles and Applications, 4th Ed.* Erlangen: Germany: Publicis Publishing, 2011.

[3] M. Ngwenyama, P. Le Roux, and L. Ngoma, "Traveling wave fault location detection technique for high voltage transmission lines," in *2021 2nd International Conference for Emerging Technology (INCET)*, 2021, pp. 1–7.

[4] O. Naidu and A. Pradhan, "A traveling wave-based fault location method using unsynchronized current measurements," *IEEE Transactions on Power Delivery*, vol. 34, pp. 505–513, 2019.

[5] L. Lessa, C. Grilo, A. Moraes, D. Coury, and R. Fernandes, "A travelling wave-based fault locator for radial distribution systems using decision trees to mitigate multiple estimations," *Electric Power Systems Research*, vol. 223, p. 109646, 2023.

[6] F. Hao, X. Yang, G. Wang, and Y. Feng, "Transmission line fault diagnosis based on machine learning," in *2023 3rd International Conference on Consumer Electronics and Computer Engineering (ICCECE)*, 2023, pp. 847–850.

[7] M. J. Davi, M. Oleskovicz, and F. V. Lopes, "An impedance-multi-method-based fault location methodology for transmission lines connected to inverter-based resources," *International Journal of Electrical Power & Energy Systems*, vol. 154, p. 109466, 2023.

[8] A. Hooshyar, M. A. Azzouz, and E. F. El-Saadany, "Distance protection of lines emanating from full-scale converter-interfaced renewable energy power plants—part ii: Solution description and evaluation," *IEEE Transactions on Power Delivery*, vol. 30, no. 4, pp. 1781–1791, 2015.

[9] F. V. Lopes, M. J. Davi, and M. Oleskovicz, "Assessment of traveling wave-based functions in inverter-based resource interconnecting lines," *Electric Power Systems Research*, vol. 223, p. 109578, 2023.

[10] M. J. Davi, R. de B. Iscuissati, M. Oleskovicz, and F. V. Lopes, "Investigating the potential of machine learning for fault location on inverter-based resource interconnection lines: Insights and recommendations," *Electric Power Systems Research*, vol. 231, p. 110366, 2024.

[11] A. Çapar and A. Basa Arsoy, "Evaluating accuracy of fault location algorithms based on terminal current and voltage data," *International Journal of Electronics and Electrical Engineering*, vol. 3, 01 2014.

[12] T. Takagi, Y. . Yamakoshi, M. Yamaura, R. Kondow, and T. Matsushima, "Development of a new type fault locator using the one-terminal voltage and current data," *IEEE Transactions on Power Apparatus and Systems*, vol. PAS-101, no. 8, pp. 2892–2898, 1982.

[13] B. Li, H. Zhao, Y. Jiang, and L. Meng, "Real-time simulation for detailed wind turbine model based on heterogeneous computing," *International Journal of Electrical Power & Energy Systems*, vol. 155, p. 109486, 2024.

[14] F. Chang, H. Sun, S. Kawano, D. Nikovski, S. Kitamura, and W. Su, "A fault detection and location technique for inverter-dominated islanding microgrids," in *2022 IEEE 5th International Electrical and Energy Conference (CIEEC)*, 2022, pp. 2041–2046.

[15] A. Jamehbozorg and S. M. Shahrtash, "A decision-tree-based method for fault classification in single-circuit transmission lines," *IEEE Transactions on Power Delivery*, vol. 25, no. 4, pp. 2190–2196, 2010.

[16] M. J. Davi, M. Oleskovicz, and F. V. Lopes, "Exploring the potential of a machine learning-based methodology for fault classification in inverter-based resource interconnection lines," *Electric Power Systems Research*, vol. 223, p. 109532, 2023.

[17] A. D. Filomena, M. Resener, R. H. Salim, and A. S. Bretas, "Distribution systems fault analysis considering fault resistance estimation," *International Journal of Electrical Power & Energy Systems*, vol. 33, no. 7, pp. 1326–1335, 2011.

[18] X. Yu, J. Gu, X. Zhang, J. Mao, and L. Xiao, "A self-adaptation non-unit protection scheme for MMC-HVDC grids based on the estimated fault resistance," *International Journal of Electrical Power & Energy Systems*, vol. 152, p. 109263, 2023.

[19] M. Hall, E. Frank, G. Holmes, B. Pfahringer, P. Reutemann, and I. H. Witten, "The WEKA data mining software: an update," *ACM SIGKDD Explorations Newsletter*, vol. 11, no. 1, p. 10–18, Nov. 2009.

[20] D. J. Mackay, "Introduction to gaussian processes," Dept. of Physics, Cambridge University, UK, 1998.

[21] D. W. Aha, D. Kibler, and M. K. Albert, "Instance-based learning algorithms," *Machine Learning*, vol. 6, no. 1, pp. 37–66, Jan 1991.

[22] J. G. Cleary and L. E. Trigg, "K*: An instance-based learner using an entropic distance measure," in *Machine Learning Proceedings 1995*, A. Prieditis and S. Russell, Eds. San Francisco (CA): Morgan Kaufmann, 1995, pp. 108–114.

[23] L. Breiman, "Bagging predictors," *Machine Learning*, vol. 24, no. 2, pp. 123–140, Aug 1996.

[24] ——, "Random forests," *Machine Learning*, vol. 45, no. 1, pp. 5–32, Oct 2001.

[25] T. K. Ho, "The random subspace method for constructing decision forests," *IEEE Transactions on Pattern Analysis and Machine Intelligence*, vol. 20, no. 8, pp. 832–844, 1998.

[26] G. Holmes, M. Hall, and E. Prank, "Generating rule sets from model trees," in *Advanced Topics in Artificial Intelligence*, N. Foo, Ed. Berlin, Heidelberg: Springer Berlin Heidelberg, 1999, pp. 1–12.

[27] R. J. Quinlan, "Learning with continuous classes," in *5th Australian Joint Conference on Artificial Intelligence*. Singapore: World Scientific, 1992, pp. 343–348.

[28] L. Breiman, "Random forests," *Machine Learning*, vol. 45, no. 1, pp. 5–32, Oct 2001.

[29] J. Quinlan, "Simplifying decision trees," *International Journal of Man-Machine Studies*, vol. 27, no. 3, pp. 221–234, 1987.

[30] A. Wiszniewski, "Accurate fault impedance locating algorithm," *IEE Proceedings C Generation, Transmission and Distribution*, vol. 130, no. 6, p. 311, 1983.